Fırat Üniversitesi Deneysel ve Hesaplamalı Mühendislik Dergisi

FUJECE

Fotovoltaik Bir Güneş Panelinin Termal Performansını Arttırmak için Deneysel ve Sayısal Uygulamalar

Murat ÇATALKAYA[1]*

[1]Teknik Bilimler Meslek Yüksek Okulu, Kahramanmaraş Sütçü İmam Üniversitesi, Kahramanmaraş, Türkiye.
[1]muratcatalkaya@ksu.edu.tr

Geliş Tarihi: 16.07.2024
Kabul Tarihi: 30.01.2025

Düzeltme Tarihi: 7.10.2024

doi: https://doi.org/10.62520/fujece.1517038
Araştırma Makalesi

Alıntı: M. Çatalkaya, "Fotovoltaik bir güneş panelinin termal performansını arttırmak için deneysel ve sayısal uygulamalar", Fırat Üni. Deny. ve Hes. Müh. Derg., vol. 4, no 2, pp. 226-244, Haziran 2025.

Öz

Son zamanlarda küresel ısınmanın etkileri, fosil yakıtlara alternatif olarak yenilenebilir enerji kaynaklarına olan ilgiyi artırmaktadır. Bu kaynaklar içerisinde güneş enerjisi, potansiyeli sebebiyle ayrı bir öneme sahiptir. Fotovoltaik (PV) paneller güneş enerjisini elektrik enerjisine dönüştürür. Fotovoltaik panellerle elektrik üretmenin en büyük sorunlarından biri, panel yüzeyine gelen enerjinin yaklaşık %80'inin ısıya dönüşmesidir. Bu dönüşüm sırasında PV panel yüzeyinde meydana gelen sıcaklık artışı panel verimliliğini olumsuz etkilemektedir. Dolayısıyla, panellerin verimli çalışabilmesi için soğutulması, çözülmesi gereken bir problem haline gelmektedir. Bu çalışmada; Kahramanmaraş iklim koşullarında monokristal PV panelin pasif soğutma üzerindeki etkilerini incelemek için sayısal analiz yöntemleri geliştirilmiştir. Öncelikle incelenecek olan fotovoltaik güneş panelinin performansı deneysel olarak araştırılmıştır. Yapılan deneylerde ortalama panel yüzey sıcaklığı 43.54°C , güneş ışınımı ve panel güçü sırasıyla 785 W/m^2, 36.32 W bulunmuştur. Daha sonra sayısal analiz için ANSYS-Fluent yazılımı kullanılmıştır. Yapılan hesaplamalı akışkanlar dinamiği (HAD) analizleri için en uygun çözüm ağı yapısını belirlemek üzere deneysel veriler kullanılmış ve Ansys programında yüzey sıcaklığı için yapılan PV panelin HAD modeli 2.44% hatayla model oluşturulmuştur. HAD modeline deneysel çalışma senaryolarında çeşitli kanat boyutları ve kanatlar arasında ki mesafenin PV panel yüzeyinde ki soğutma ya olan etkili incelenmiştir. HAD analizleri sonucunda kanat geometrisine nazaran, kanatlar arasında ki mesafede ki yaklaşık %40 lik (5mm) artışta kanat uç sıcaklığında yaklaşık 4°C bir azalma elde edilmiştir.

Anahtar kelimeler: Monokristal güneş paneli, Kanatçık, HAD, PV panel, Isı transferi

*Yazışılan Yazar

İntihal Kontrol: Evet – Turnitin
Şikayet: fujece@firat.edu.tr

Firat University Journal of Experimental and Computational Engineering

Experimental and Numerical Applications to Increase Thermal Performance of a Photovoltaic Solar Panel

Murat ÇATALKAYA [1*]

[1]Vocational School of Technical Sciences, Kahramanmaraş Sütçü İmam University, Kahramanmaraş, Turkey.
[1]muratcatalkaya@ksu.edu.tr

Received: 16.07.2024
Revision: 7.10.2024
Accepted: 30.01.2025
doi: https://doi.org/10.62520/fujece.1517038
Research Article

Citation: M. Çatalkaya, "Experimental and numerical applications to ıncrease thermal performance of a photovoltaic solar panel ", Firat Univ. Jour.of Exper. and Comp. Eng., vol. 4, no 2, pp. 226-244, June 2025.

Abstract

Recently, the impact of global warming has intensified interest in renewable energy sources as alternatives to fossil fuels. Among these resources, solar energy stands out due to its potential. Photovoltaic (PV) panels play a crucial role in converting solar energy into electrical energy. However, one of the biggest challenges in generating electricity with PV panels is that approximately 80% of the energy from the panel surface is transformed into heat. This temperature increase on the PV panel surface negatively affects its efficiency, making it essential to find effective cooling solutions. In this study, we developed numerical analysis methods to investigate the effects of monocrystalline PV panels on passive cooling under the climatic conditions of Kahramanmaraş. First, we performed experimental investigations to assess the performance of the photovoltaic solar panels. The experiments revealed an average panel surface temperature of 43.54°C, with solar radiation and panel power measuring 785 W/m² and 36.32 W, respectively. We then employed ANSYS Fluent software for numerical analysis. The experimental data were utilized to determine the most suitable solution network structure for computational fluid dynamics (CFD) analyses, resulting in a CFD model of the PV panel with a surface temperature error of just 2.44%. The CFD model was used to examine how different fin sizes and distances between fins affected cooling on the PV panel surface. The CFD analysis indicated that increasing the distance between the fins by approximately 40% (5 mm) led to a reduction of about 4°C in fin tip temperature compared to the original fin geometry.

Keywords: Monocrystalline solar panel, Heatsink, CFD, PV panel, Heat transfer

*Corresponging author

1. Introduction

Today, the increase in energy demand obtained from fossil fuels increases the interest in renewable energy sources as an alternative to fossil fuels. Among these sources, Solar energy, which stands out with its unlimited energy potential, has a significant place [1]. Solar energy is collected with the help of thermal panels or solar collectors and is used for many purposes. One of the common uses of solar energy is its direct conversion into electrical energy. Photovoltaic (PV) panels are used for this conversion. To use PV panels efficiently, it is necessary to determine their operating conditions well. The efficiency of PV panels depends on factors such as surface contamination, shining, the panel's position relative to the sun, cell type, and temperature [2]. PV panels absorb a significant portion of the energy from the sun. However, Only 15-20% of this energy, given out as heat, can be converted into electrical energy [3]. As the PV panel collects energy from the sun, the temperature on its surface increases. This negatively affects the panel's electricity production and reduces its efficiency. Therefore, for PV panels to become more efficient in electricity production, dissipating the heat on their surfaces becomes a problem that needs to be solved [4-5]. Various methods exist to solve the cooling problem of reducing the surface temperature of PV panels [6]. These are active cooling and passive cooling strategies. Active cooling converts a coolant into intermediate fluid using mechanical heat pipes or pumps [7]. In passive cooling, another cooling technique, heat is removed from the hot surface only by natural heat transfer without an active component [8-9]. Air-cooled fins are often preferred in the passive cooling method. The heat on the fins is evacuated from the system by passing to the air filtering through them. Thanks to these fins placed on the bottom surface of the PV panel, the heat transfer surfaces are increased, and the cooling capacity is increased [10]. It is essential to determine an effective cooling method for PV panels and to design them according to this method. In this context, experiments must be conducted after going through various experimental setups' design and manufacturing processes for the specified cooling systems. This requirement is a challenging process to overcome in terms of time and cost. These processes can be more efficient thanks to programs that perform computational fluid mechanics (CFD) analysis. Thanks to CFD programs, the behavior of systems is observed by analyzing them under various scenarios at the design stage before reaching the manufacturing stage [11].

The main goal of this research is to increase the efficiency of a monocrystalline PV panel under passive cooling by using a heatsink with specific parameters under Kahramanmaraş's climatic conditions. For this purpose, experimental studies were conducted in the ambient temperature range of 25-55 °C. Based on the data obtained from experimental studies, the panel's CFD model was created using the Ansys program. Fins of various sizes were applied to the CFD model, and temperature distributions were observed on the panel surface. With the help of CFD analyses supported by experimental parameters, the effects of the change between blade spacing, blade thickness, and blade height on PV panel surface cooling were examined.

2. Passive Cooling and Heatsink

Passive cooling methods, which operate without additional energy input, are simple yet effective in enhancing heat transfer through natural convection to cool PV panels. In passive cooling, the heat is effectively transferred from the heat source, such as a PV panel, to the outside air and then distributed to the environment. The three main categories of passive cooling techniques, namely passive air cooling, passive water cooling, and passive conductive cooling, are all simple to implement [12]. This study specifically focuses on the simplicity of passive air cooling and using a heatsink. Thermal fins, a simple and cost-effective solution for cooling PV panels, require minimal maintenance and consume no electricity. A heatsink, typically made of metal, is designed to significantly increase heat transfer from its source to the surroundings through natural or forced convection [13-15]. It is engineered to enhance heat dissipation and contact area with ambient air for efficient heat transfer. Natural convection, which occurs when cooling air moves across the fin array due to pressure or temperature differences, further enhances the simplicity of these techniques. Optimal heat transfer is achieved within a limited spacing range for high fins, whereas shallow fins benefit from a more extensive range [16-17]. To identify the most effective fin design, it is essential to conduct a heat transfer analysis for the simplest case. Figure 1 beautifully illustrates a surface adorned with a single fin, radiating heat into the surrounding air through unforced convection. Here, T_{∞}-air signifies the air temperature, complemented by the air convective heat transfer coefficient [18].

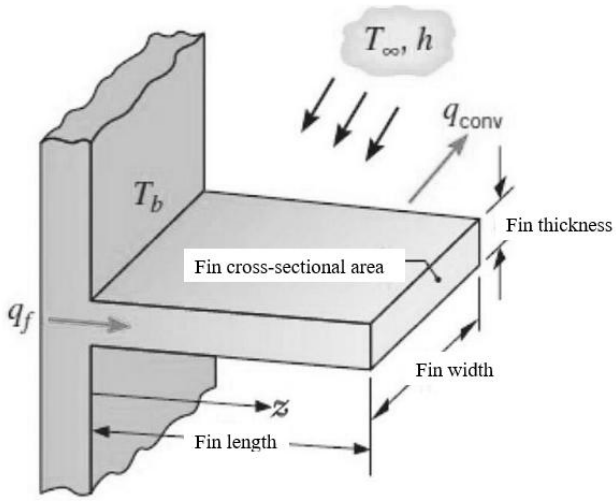

Figure 1. Surface with one fin [18]

Using the equations below, the total amount of heat to be transferred through the fins and its parameters can be calculated [18]. Equation 1 is expressed as the most general form of the total heat transfer relationship from the fin surface [19].

$$Q_T = Nq_f + \bar{h}A_b\Delta T \tag{1}$$

where A_b is non-finned surface (the base of the heat sink where there are no fins), Fourier's law is applied to the base of the fin to obtain q_f, and N is the total number of fins. Here, $\bar{h}$ is the total convection heat transfer coefficient transferred from the fin surface and is calculated by Eq.2.

$$\bar{h} = \frac{\overline{N_{uH}}k_a}{H} \tag{2}$$

where N_{uH} is the Nusselt number and represents the dimensionless temperature gradient on the fin surface. The thermal conductivity of air at a given temperature is represented by k_a. H is the definitive characteristic length of the system. $\overline{N_{uH}}$ is explicitly defined in terms of other Rayleigh and Prandtl numbers, as demonstrated in Eq. 3.

$$\overline{N_{uH}} = (Ra, Pr) \tag{3}$$

In Eq.3, Ra is Rayleigh and Pr is Prandtl number. Prandtl number as the ratio of momentum and thermal dissipations is defined. Rayleigh number is a dimensionless number that characterizes heat transfer in natural convection events. When the necessary simplifications are made, the heat transfer that will occur through a fin is obtained with the Ra number relation given in Eq. 4.

$$Ra = \frac{g\beta(T_b - T_\infty)H^3}{v^2}.\frac{v}{\alpha} \tag{4}$$

At the junction between the heat sink and the PV panel, there is a resistance to heat transfer due to small air pockets between the surfaces. This resistance is reduced by using thermal interface materials (TIMs) to improve interface contact and reduce thermal resistance [18]. To provide effective passive cooling through the heatsink, materials with high thermal capacity and conductivity transfer thermal energy from the heat source and distribute heat efficiently to the environment. Aluminum alloys are commonly used for heatsinks

due to their favorable properties. Still, copper offers superior properties but requires unique manufacturing processes, such as milling, due to less forming properties or difficulty in machining operations. Typically, copper is also used by integrating it into the heatsink base, onto which aluminum fins are attached [20-21]. Heatsinks have emerged as a cornerstone in thermal management, celebrated for their versatile geometric designs. Among these, plate and pin shapes stand out as the most effective choices, balancing exceptional performance with cost efficiency and ease of production. The literature frequently highlights several fin types that excel in these applications, including the elegant Plate Fin, the robust Square Pin Fin, the efficient Round Pin Fin, and the innovative Stepped Round Pin Fin, all of which are beautifully illustrated in Figure 2.

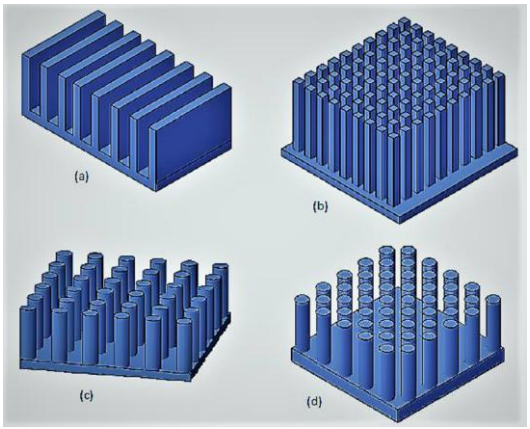

Figure 2. Various types of Heatsink; (a) Plate Fin (b) Square Pin Fin (c) Round Pin Fin (d) Stepped Round Pin Fin [22]

In a medium with limited thermal conductivity, as well as when heat is transferred to a large area, the distribution resistance must be taken into account, as it can lead to significant temperature gradients and uneven heat distribution [18].
It's important to note that uneven heat distribution, where some fins have lower temperatures than others, is a situation that needs to be avoided. Achieving even heat distribution is a key goal in the design and maintenance of PV panel systems, and this can be facilitated by strategies such as thickening the fin base.
Additionally, the effectiveness of a heat fin is important to note, which is greatly affected by the configuration of the PV panel system, including factors such as local climatic conditions, wind speed, and direction, solar panel height, orientation, fin geometry, etc. [21]. To achieve the cooling effect, increase the heat transfer from the back side of the PV panel [23]. Although increasing the thermal conductivity of the back sheet is one approach to achieve a cooling effect of up to 0.07°C, alternative methods need to be investigated [24]. Fourier's law of heat transfer is clear. Accordingly, assuming that the temperatures of the surroundings and the heat-radiating body are constant, the cooling effect can be increased by using a pump or fan to increase convection or by expanding the heat-radiation area to the surroundings [25]. This situation can be achieved using fins with additional rectangular or pin-shaped surfaces. It was carried out with the assumption that for every 1 °C increase in temperature on the PV panel, the electrical efficiency of the PV panel module decreases by 0.5% [26-27]. The effect of temperature on PV panel performance can also be explained as follows: PV panels start producing electricity when they receive radiation from the sun. While some of the radiation coming from the sun turns into electrical energy, some of it emerges as heat energy. This event causes the PV cells to heat up. As the PV cells heat up, the short circuit current (I) of the PV modules increases, while the open circuit voltage (V) decreases and thus the electrical efficiency decreases (Figure 3). Therefore, the cooling effect is significant for the PV panel.

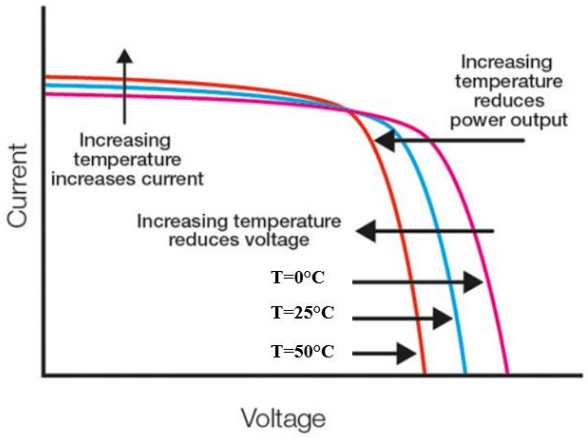

Figure 3. Effect of operating temperatures on PV panel performance [28-29]

3. Material and Methodology

To design an effective heatsink, modern approaches to design must be applied. These contemporary approaches require determining the temperature distribution characteristics of the designs and making designs considering these features. It is essential to conduct experimental studies to observe or evaluate the effectiveness of design results. However, experimental studies are methods that require both time and cost. In addition, situations such as lack of equipment and limited opportunities occur in experimental studies. For all these negative reasons, CFD simulation programs are used. By performing virtual modeling using experimental conditions in CFD simulations, high-quality solutions are obtained for the behavior of designs under flexible physical conditions [30]. Thus, it saves time and experimental expenses [31-32]. In this study, experimental studies were carried out under passive cooling conditions using monocrystalline panels to test the accuracy of CFD analyses and determine the PV panel's characteristic properties. Experimental study results: CFD simulations were used to numerically simulate the heat distribution on the panel and the cooling effect of the fins on the panel. Fin analysis in 9 different sizes was performed in the CFD environment. As a result of CFD studies, fin dimensions, adequate fin spacing, fin thickness, and distance between fins on the fin surface temperature distribution were determined.

3.1 Material

3.1.1. Solar panel module

The solar panel examined in this study is a monocrystalline module produced by Uretech company that can produce 50 W (watt peak) power. Table 1 shows the features of the solar panel module used in the study.

Table 1. Solar module features

Features	Values
Photovoltaic Panel	Mono-crystalline 159x39 mm
Number of Cells	36
Open-Circuit Voltage (VOC)	24.62 V
Short-Circuit Current (ISC)	2.57A
Maximum Power (PMPP)	50W
Operating Temperature Range	-20°C / 80°C
Dimensions	662x159x25mm

In Figure 4, the solar panel is designed in layers. Each layer used serves a different purpose. At the top, the panel used Ethylene Tetrafluoroethylene (ETFE) instead of tempered glass. ETFE was chosen due to its low

weight, higher transparency, and ability to make the laminated panel flexible. ETFE cells are free of dirt, etc. It serves the purpose of protection from external factors. Underneath the ETFE layer, it was used as a protective base on which a thin layer of Ethylene-Vinyl Acetate (EVA) was spread. EVA is a specially manufactured material used to bond the panel layers together. This bonding process is done using the lamination technique. The cells were placed between two EVA sheets, with dimensions of 159x39 mm and 36 cells. Under the EVA layer under the cells is a Polyethylene Terephthalate (PET) layer made of insulated plastic material. On the bottom layer of the panel, other layer series are fixed with a frame on a Carbon Fiber Composite Polymer (CFRP) plate. An aluminum frame was placed around the layers to hold all the layers together.

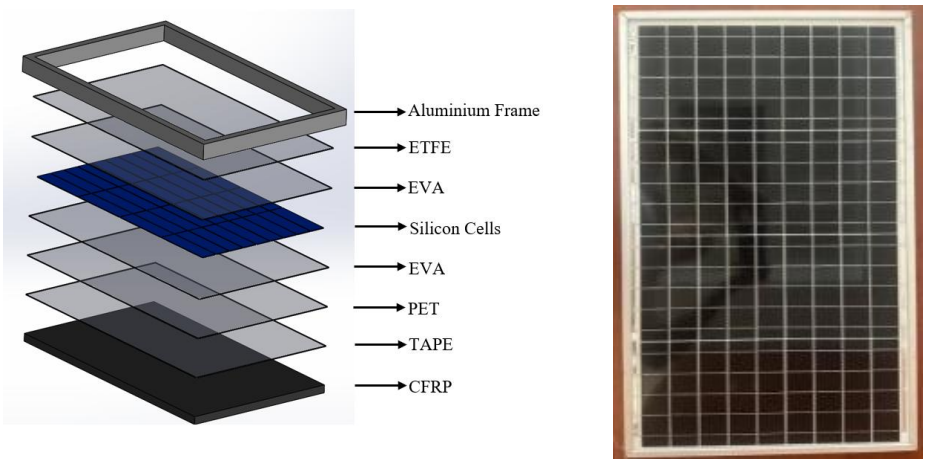

Figure 4. View of the layers of the monocrystalline PV Solar Panel used in the study

3.2. Method

The study covers two methods. The first of these is experimental studies to determine the characteristic features of the PV panel and to determine the accuracy of CFD analyses.

The second method is CFD analysis. ANSYS was used as the CFD program in numerical methods. Ansys models the system using fluid mechanics equations as well as heat and mass flow with finite element analysis.

3.2.1 Experimental procedure

This study presents a thoughtfully designed experimental setup aimed at gathering insightful data and evaluating the performance of a solar panel. At the heart of the experiment is a high-quality monocrystalline photovoltaic (PV) panel. The panel's positive and negative terminals were expertly connected to a data acquisition socket via a robust cable, allowing for precise measurement of current and voltage. For this purpose, an ammeter was utilized to capture the DC current, while a voltmeter ensured accurate voltage readings.

In addition to the monocrystalline panel, the experimental design featured a 50 W polycrystalline PV panel, complemented by a multimeter to facilitate current and voltage measurements. To enrich the study even further, instruments were employed to monitor essential meteorological parameters, including temperature, air velocity, and solar radiation. This comprehensive approach not only underscores the rigor of the investigation but also enhances our understanding of solar panel performance under varying conditions.The panel in the experimental set is placed on the ground in such a way that it receives the sun's rays in the best way during the day. A dummy load of 2.5 ohms was included in the panel to obtain the current draw generated from the PV panel. The measurements required for the study were determined by manual readings every hour. To measure the power generated by the PV panel system, current-voltage values were obtained by

observing the multimeter display connected to the dummy load. Figure 5 shows the schematic of the experimental setup.

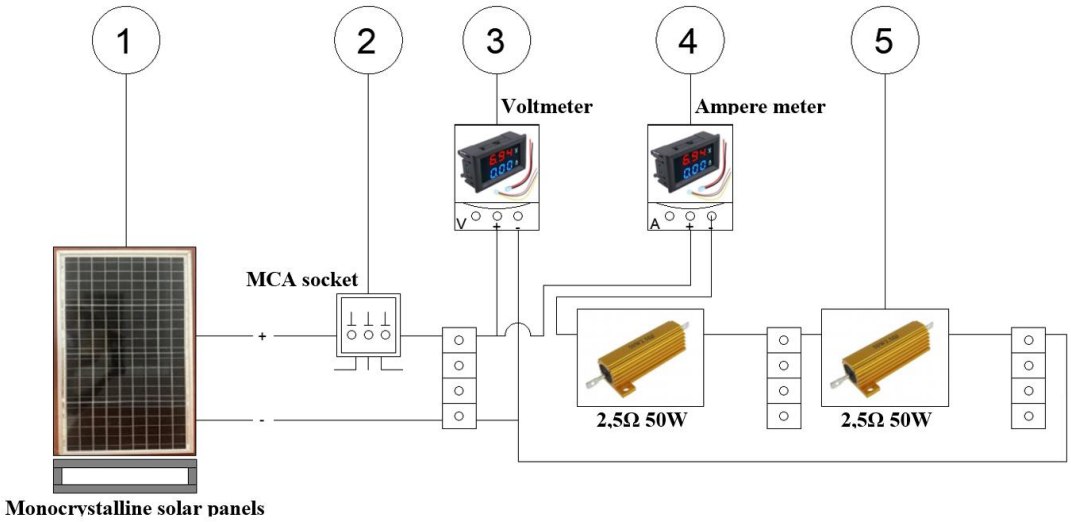

Figure 5. Schematic view of the experimental system.

This research used a monocrystalline PV solar panel measuring 622 × 393 × 20 mm. A precision Testo 875-2 irradiance meter was used to measure incident solar radiation. To measure the temperature and average temperature of the PV panel, it was monitored for a certain period using an infrared laser thermometer with a sensitivity of ±2°C, model Uni-T UT306. The wind speed under the PV panel was measured using an anemometer with a Testo 405-V1 model sensitivity of ±0.1 m/sec and a measurement range of 0 … 10 m/sec (0 … +50 °C).

Furthermore, the comprehensive performance of the PV panel was measured by recording the instantaneous power, current and voltage values . This was done using a Wattmeter, Ammeter and Voltmeter, which are standard devices for such measurements. The devices used and the experimental process are shown in Figure 6.

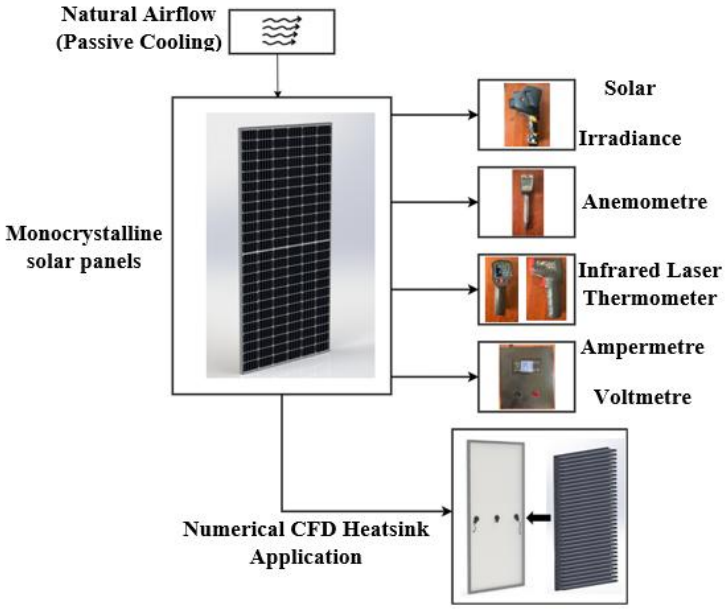

Figure 6. Experimental setup schematic configuration of PV panel

As shown in Figure 6, an infrared laser temperature meter was used to measure the surface temperature of the PV panel. An Anemometer was used to measure the speed of the air passing around the panel and a Solar Irradiance Meter was used to measure the radiation reaching the surface. In addition, a wattmeter was used to measure the amount of power that was generated by the panel during the experiment.

3.2.2 Numerical analysis procedure

In this section, numerical studies have been carried out to analyze the convective heat transfer of the PV panel and the heatsink to be placed on the bottom surface of the panel. Numerical studies were carried out in Ansys Fluent as steady-state CFD analysis. Since this analysis was performed to investigate thermal changes for conditions over a certain period of time, steady-state thermal analysis was chosen.

PV panel

In this study, geometry models were created in 6 layers, each 662x393 mm, using Ansys's Design Modeler Module. The cells in the PV panel are rectangular, with dimensions of 159x39 mm, and are modeled as 36 pieces. The appropriate material type and thickness of the layers used in the numerical study are given in Tables 2 and 3. In the analysis, the connected contacts that allow complete transfer of heat between layers were modeled by taking into account.

Table 2. Properties of the layers of the PV panel [33]

Layer	Material	Layer thickness(mm)
1	ETFE	0.28
2	EVA1	0.20
3	Silicon	0.15
4	EVA2	0.20
5	PET	0.20
6	Tape	0.13
7	CFRP	2.00

Table 3. Physical and thermal properties of the materials selected for the layers of the PV panel [33]

Material	Density (kg/m^3)	Thermal conductivity (W/(m·K))	Specific heat (J/(kg·K))
ETFE	1730	0.24	1172
EVA	945	0.35	2090
Silicon	2330	148	700
PET	1350	0.275	1275
Tape	1012	0.19	2000
CFRP	2770	177	875

The intricate 3D models essential for performing CFD analyses of the PV panel utilized in the experiments are elegantly showcased in Figures 7 and 8. The thermal fin model is shown in Figure 7a. Figure 7b shows the geometry consisting of PV panels without thermal fins. Figure 8 shows the dimensions of the PVC panel used and the cells on the panel.

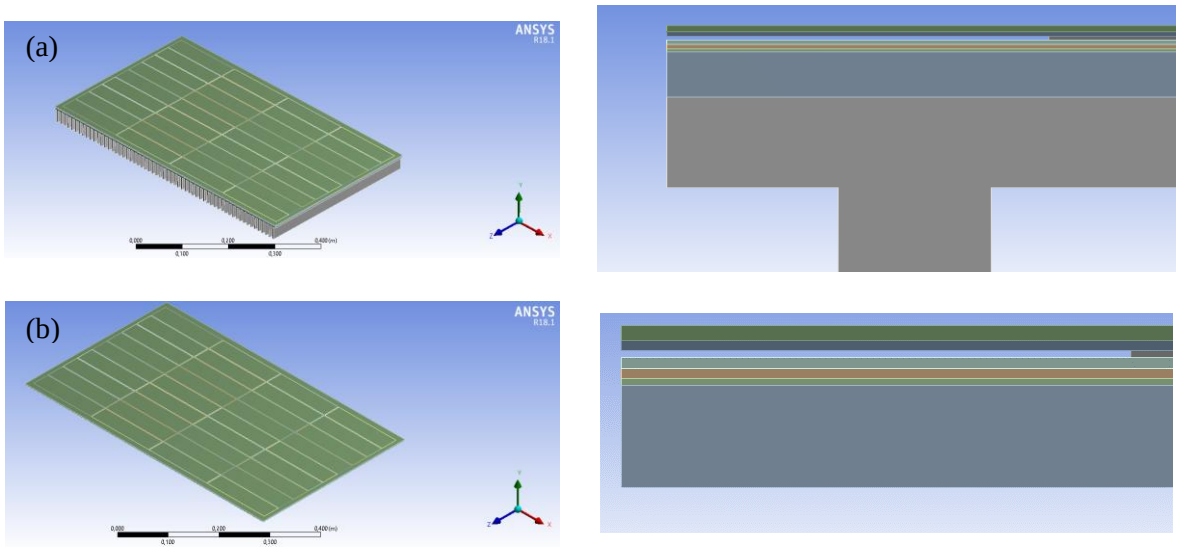

Figure 7. (a) PV panel with fin and (b) without thermal fins

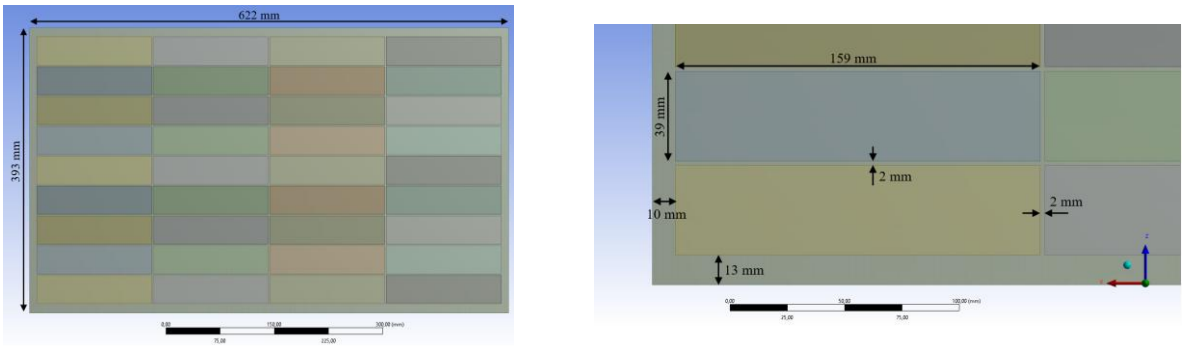

Figure 8. PV panel geometry

Heatsink

In order to examine the effect of fin height, fin width and distance between fins on heat transfer, three different levels were determined for each parameter during design and other parameters were kept constant. In the finite element analyses, three different blade heights (30 mm - 40 mm - 50 mm), two different blade widths (4 mm - 7 mm) and two different distances between blades (7 mm -12 mm) were determined as variable parameters. Table 4 shows the experimental design set and dimensional values.

Table 4. Dimensions of fins

Model name	(mm)	b (mm)	w(mm)
HS3047	30.00	4.00	7.00
HS3077	30.00	7.00	7.00
HS30712	30.00	7.00	12.00
HS4047	40.00	4.00	7.00
HS4077	40.00	7.00	7.00
HS40712	40.00	7.00	12.00
HS5047	50.00	4.00	7.00
HS5077	50.00	7.00	7.00
HS50712	50.00	7.00	12.00

As seen in Table 4, the fin height is indicated by h, the finspan is indicated by b and the distance between fins is indicated by w. The geometries of the finlets are given in Figure 9. CFD analyzes of the fins were carried out only for the regions where the maximum temperature of the PV panel was achieved [18].

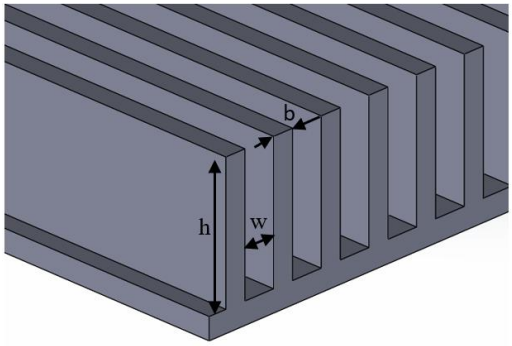

Figure 9. Fin geometry

Mesh structure

For the numerical solution, the network model was created as a multizone. Network models were created in three different sizes: Model-1, Model-2, and Model-3, respectively, with the dimensions used in the network sensitivity study being 2.5 mm, 3.5 mm, and 4.5 mm. Network sizes are not uniform across the solution domain. In CFD simulations, the solutions' accuracy, rapid convergence, and stability largely depend on the network quality. Mesh quality is defined by many methods, the most common of which is the skewness value. Generally, skewness is a function of the angle between any two sides forming the cell. In CFD studies, the skewness value should be below a maximum of 0.95 and the orthogonal quality value should be greater than 0.15 [34]. Detailed information about the dimensions of the solution network structure is given in Table 5. Table 5 gives skewness and orthogonal quality values for 3 different models. It is clearly seen that the quality values for all three models are within acceptable limits. The image obtained after the mesh process is given in Figure 10.

Table 5. Mesh statistics

Model number	Number of elements	Maximum mesh size (mm)	Average skewness value	Maximum skewness value	Average orthogonal quality value
Model-1	581964	2.5	5.76e-002	0.63	0.96
Model-2	316271	3.5	8.74e-002	0.85	0.94
Model-3	141904	4.5	3.28e-002	0.58	0.98

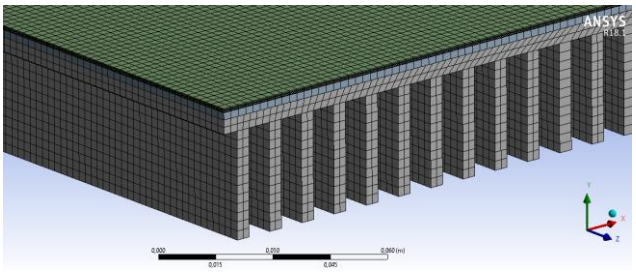

Figure 10. 3D MESH Model domain

Boundary conditions

In this study, the boundary conditions used for the numerical CFD analysis of the PV Panel can be summarized as follows: The airflow is 3D, and analyses were performed at constant temperature. Air

temperature was obtained from experimental data for a specific day and time. Air distribution on the PV panel is the same everywhere. Side surfaces are entirely insulated. The radiation boundary condition for the upper surface is defined. k-e was chosen as the turbulence model, and the turbulent viscosity ratio is 5% and 10%, respectively. The flow is assumed to be incompressible. The analyses were solved by considering steady-state conditions for specific hours during the day. The boundary condition in the outlet region is defined as the pressure outlet. The boundary conditions in the study were handled in accordance with the experimental conditions. The experimental studies were carried out in accordance with the PV panels used in the industry.

For the CFD analysis, we employed the powerful mesh-based ANSYS. This tool facilitated a comprehensive analysis of the numerical data by dividing the model into simpler regions [35]. The study involved solving the Navier-Stokes (N-S), energy, continuity, and turbulence equations numerically, under the specified boundary conditions, to simulate the heat transfer process between the air and the fin [36]. CFD solution equations used in numerical analysis are Equations. It is given in Equations 5-12.

N-S equations in x, y and z directions can be expressed in Eq.5-7.

$$\nabla(\rho.\vec{U}.u) = -\frac{\partial p}{\partial x} + \frac{\partial \tau_{xx}}{\partial x} + \frac{\partial \tau_{yx}}{\partial y} + \frac{\partial \tau_{zx}}{\partial z} \tag{5}$$

$$\nabla(\rho.\vec{U}.v) = -\frac{\partial p}{\partial y} + \frac{\partial \tau_{xy}}{\partial x} + \frac{\partial \tau_{yy}}{\partial y} + \frac{\partial \tau_{zy}}{\partial z} \tag{6}$$

$$\nabla(\rho.\vec{U}.w) = -\frac{\partial \mathrm{p}}{\partial \mathrm{z}} + \frac{\partial \tau_{xz}}{\partial \mathrm{x}} + \frac{\partial \tau_{yz}}{\partial \mathrm{y}} + \frac{\partial \tau_{zz}}{\partial \mathrm{z}} \tag{7}$$

Here ρ is the density of the fluid, (u, v and w) are the velocity components in three directions, U is the air velocity, τ is the viscous stress tensor and p is the pressure.

The energy equation in Eq.8 is;

$$\nabla(\rho.h.\vec{U}) = -p\nabla\vec{U} + \nabla(k\nabla T) + \delta + S_h \tag{8}$$

In Eq.8, h represents the total enthalpy, δ denotes the dissipation term, k signifies the thermal conductivity, T stands for the temperature, and S_h indicates the thermal source term.
The continuity equation in Eq.9 is;

$$\nabla(\rho.\vec{U}) = 0 \tag{9}$$

The turbulence solver realizable k-ε equations used in this study are given below in their general form [35-37].

Turbulence Kinetic Energy (k) equation in Eq.10;

$$\frac{\partial}{\partial x_j}(\rho k u_i) = \frac{\partial}{\partial x_\mathrm{l}}[(\mu + \frac{\mu_t}{\sigma_k})\frac{\partial k}{\partial x_i}] + G_k + G_b - \rho\varepsilon \tag{10}$$

Loss Rate (ε) equation in Eq.11;

$$\frac{\partial}{\partial x_i}(\rho\varepsilon u_i) = \frac{\partial}{\partial x_j}\left[(\mu + \frac{\mu_t}{\sigma_\varepsilon})\frac{\partial \varepsilon}{\partial x_i}\right] + \rho C_1 - \rho C_2 \frac{\varepsilon^2}{k + \sqrt{v\varepsilon}} + C_{1_\varepsilon}\frac{\varepsilon}{k}C_{3_\varepsilon}G_b \tag{11}$$

Turbulence viscosity equation in Eq.12;

$$C_1 = max\left[0.43, \frac{\eta}{\eta + 5}\right], \rightarrow \eta = S\frac{k}{\varepsilon}, \rightarrow S = \sqrt{2S_{ij}S_{ij}} \tag{12}$$

The constant values used in the turbulence model of this study are as follows;

$(C_{1\varepsilon} = 1.44), (C_2 = 1.9), (\sigma_k = 1.0)(\sigma_\varepsilon = 1.2)$

4. Result and Discussion

4.1. Experimental result

Experiments with monocrystalline PV panels were carried out in Kahramanmaraş province, under passive cooling, in May, and solar radiation values varying according to hours are shown in Figure 11. Measurements were made between 9:00 and 17:00 local time, and the highest radiation values of 1010 W/m2 were recorded at noon. In the calculations, the maximum radiation value falling on the PV panel was accepted as 1000 W/m2. The airspeed passing over the panel surface was recorded as 0.46 m/s during the experiments.

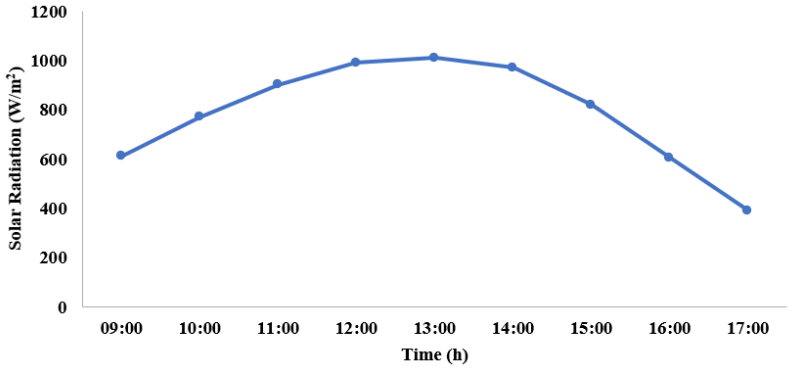

Figure 11. Kahramanmaraş solar radiation values varying according to hours in May

Figure 12 shows the variation graph of the surface temperatures of the PV panel under passive cooling throughout the day. As seen in the graph, the surface temperature of the panel reached a maximum of 50.856°C under passive cooling at around 13:00, when the temperature reached its highest level.

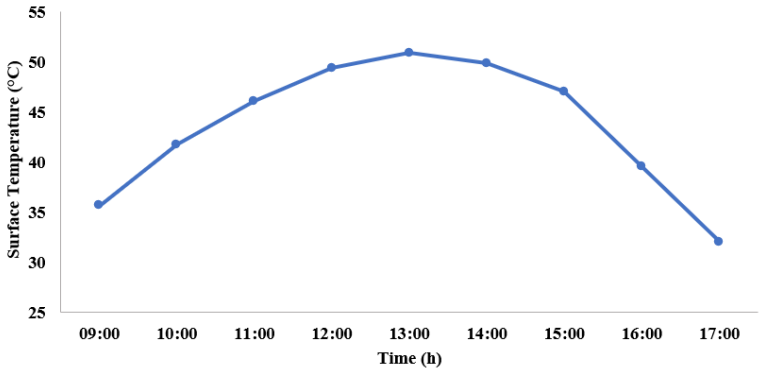

Figure 12. Change graph of surface temperatures of the PV panel under passive cooling throughout the day

Figure 13 shows the Current-Voltage and Power-Voltage characteristics of the PV Panel in a horizontal position under Passive air cooling, where the airspeed is 0.46 m/s. As seen in Figure 12, the current-voltage change at different operating temperatures can be seen. It is clearly seen that the voltage changes are inversely proportional to the increase in working surface temperature between 25°C and 55°C. For the PV panel used in the experimental system, the voltage drops approximately 0.3V for every 1°C temperature increase. As seen in Figure 12, it is clear that the PV panel used in the experiment reached maximum power at 25°C operating conditions. Power production varies inversely with the increase in temperature. In the experiments,

it is clearly seen that temperature is among the critical factors affecting the efficiency of monocrystalline PV panels.

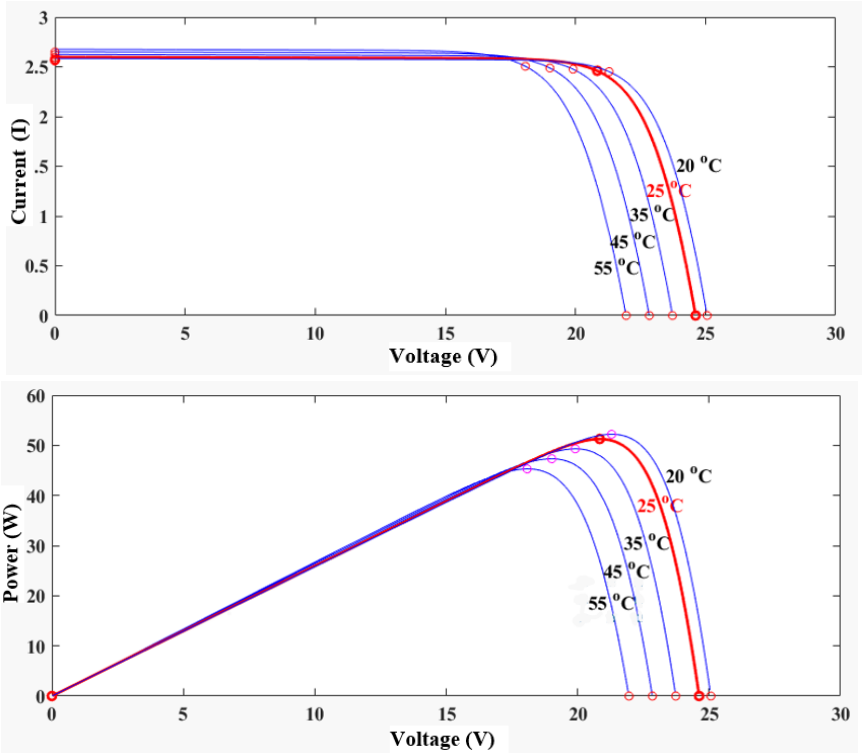

Figure 13. Current-Voltage and Power-Voltage characteristics of the PV Panel in horizontal position, under Passive air cooling where the air speed is 0.46 m/s

4.2 Numerical analysis result

This section includes the findings of thermal numerical studies to analyze the convective heat transfer of PV panels and a heatsink to be placed on the bottom surface of the panel. The study applied the network density test to select the optimum node and element sizes to obtain a reliable solution independent of the network size. A mesh density test was conducted for the PV panel to see the effect of the change in mesh size on the PV panel surface temperature at different times (Figure 14).

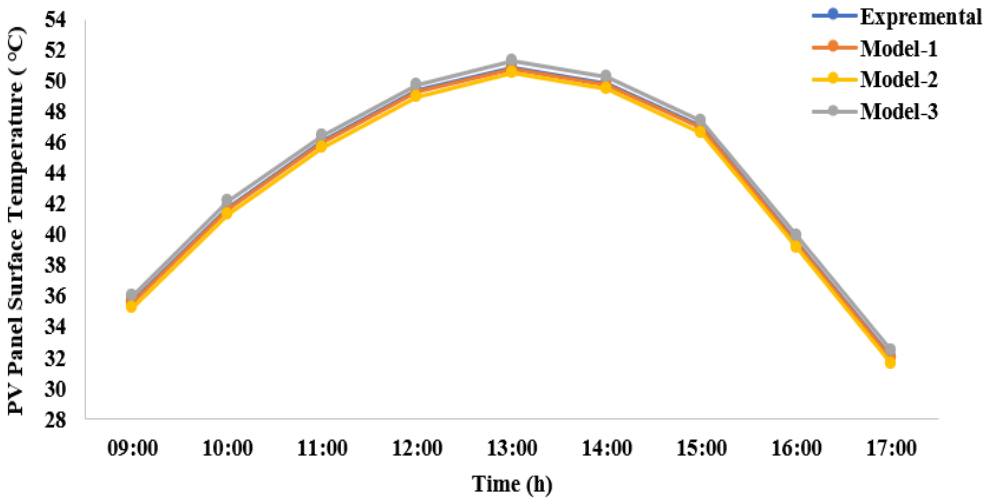

Figure 14. Graph showing the effect of mesh size on PV panel surface temperature at different times

In Figure 14, we observe a change in the mesh number from Model-1 fine size to Model-3 coarser size. This meticulous alteration affects the convergence of the PV Panel to the surface temperature. Despite this, all three models demonstrate a high degree of compatibility with the experimental results at specific time intervals. The error rate between the analysis in the mesh model created using Model-1 and the experimental data is less than 2.4%, a testament to the thoroughness of our simulation process.
Figure 15 (a) shows the temperature contours obtained to simulate the panel temperature under passive cooling at the desired boundary conditions of the PV panel for an air temperature of 32°C at 13:00. It is seen that the panel temperature varies around 49°C on the top and middle surface of the silicon cell layer responsible for electricity generation. The maximum cell temperature was obtained as 49.615°C. Experimentally, the max. The temperature was obtained as 50.856°C. Figure 15 (b) shows the temperature contours in the bottom CFRP layer as a result of simulating the panel temperature under passive cooling at the desired boundary conditions for the PV panel at 13:00. It is clearly seen that the temperature changes around 48°C on the upper and middle surface of the CFRP layer. Its maximum temperature was obtained as 48.837°C. Experimentally, the max. The temperature was obtained as 47.4°C.

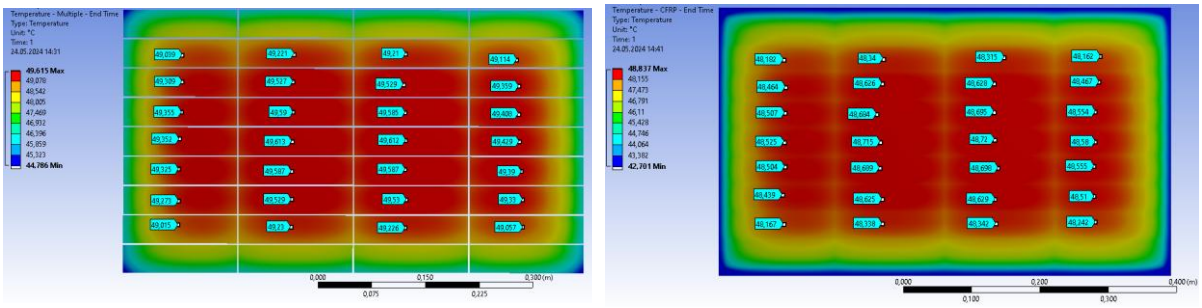

(a) **(b)**

Figure 15. (a) Temperature contours of the PV panel under passive cooling for 32°C air temperature at 13:00; (b) Temperature contours on the CFRP layer of the PV panel under passive cooling at 13:00

Numerical analysis studies of the fins were carried out based on the temperature distribution of the CFRP layer, which is the bottom layer of the PV panel. To obtain the temperature fields, CFD analyses of nine different heatsinks were simulated in the ANSYS FLUENT program (Figure 16). The CFD analysis calculates the average heat flux on the bottom region of the heatsink and the bottom surface of the PV panel, based on thermal analysis results. In addition to heat flux, the simulation also considers factors such as solar radiation and natural convection heat transfer to the fins. As illustrated in Figure 16, HS50712 features the longest blade length and the widest gap between the blades.

The fin model for HS50712 elegantly extends over a broader area, a testament to the influence of spreading resistance. In an intriguing comparison of temperature values at the tips of the finlets, the HS50712 model stands out with the lowest temperature, measured at a remarkable 300.2 K. Furthermore, the most striking temperature gradient between the base and tip is observed in the HS50712 fin model, showcasing its impressive thermal performance.

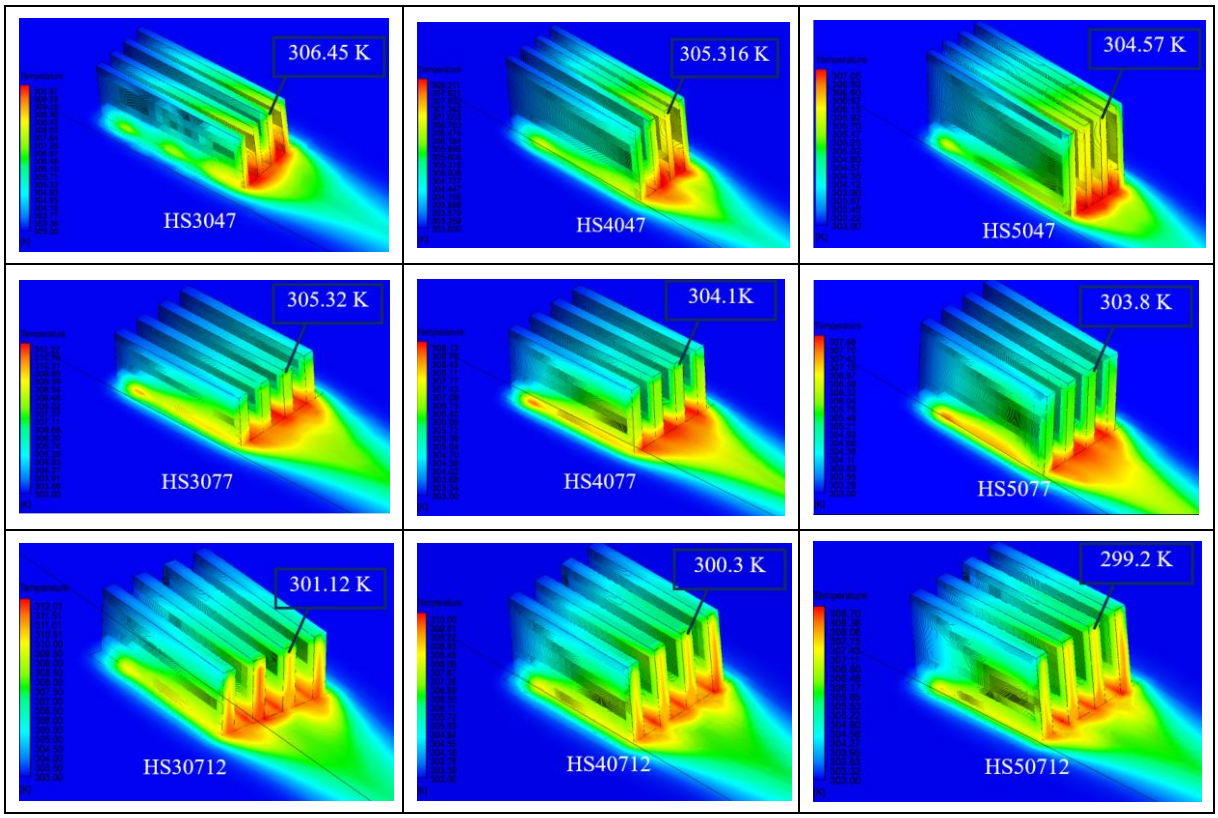

Figure 16. CFD analyzes nine different heatsinks to obtain temperature fields

In PV panels, 1°C change in surface temperature affects the panel efficiency by 0.5 [27]. As a result of the study, a cooling of 4°C is provided by optimizing the size of the fins placed on the bottom surface of the panel. In this case, an efficiency increase of 2% is achieved. Compared to similar studies in the literature, Amrizal et al. obtained a cooling of 1.25ºC by changing the blade thickness and Reynolds number on the Pv panel [38]. Jing et al. obtained a 2°C decrease in surface temperature by changing the gaps between the blades [39].

5. Conclusion

In this study, experiments were carried out under Kahramanmaraş conditions using a monocrystalline PV solar panel, and the operating characteristics of the panel were determined. As a result of the experimental study, the panel efficiency used in the system examined was 1000 W/m2, while the thermal efficiency was obtained as 16.2%. This efficiency is clearly seen in the panel characteristic curves, where it decreases with increasing surface temperature of the panel surface. According to the data from the experiments, a 3D model of the PV panel was developed using ANSYS simulation software, and various CFD analyses were performed. The properties of the actual PV panel material, such as layer density, thermal conductivity, and specific heat capacity, created the CFD model of the panel. The PV panel model was simulated under the climate condition of Kahramanmaraş, where the ambient temperature at 13:00 was fixed at 32°C.

The experimental and simulation results in this study successfully converged, with a small error value of 2.4%. This convergence, a testament to the accuracy of the research process, was crucial in understanding and addressing the decrease in efficiency due to increasing surface temperature of the panel. To tackle this issue, CFD studies were conducted using the ANSYS program, ensuring the reliability of the findings.

In the CFD studies, heatsinks were applied to the PV panel to reduce the surface temperature under passive cooling. In the study, nine different heatsink sizes were used, and their thermal behavior was examined. The effect of the change in the size of the finlets was determined based on the temperature values at the fin tips. As a result of CFD analysis, it was observed that for the same fin width and distance between the fins, an

approximately 40% (10 mm) increase in fin height decreased the fin tip temperature by approximately 2°C. An increase of approximately 40% (3mm) in fin thickness showed a decrease of 1.16°C in tip temperature. With an increase of approximately 40% (5mm) in the distance between the fins, a decrease of approximately 4°C in fin tip temperature was achieved. As a result of the analysis, the lowest temperature value was obtained at 299.2K using the HS50712 fin type. In the future planning of this study, the most effective fin type for PV panel surface cooling will be produced as a result of numerical analysis, and surface temperatures and energy production performance will be investigated. The results will be compared with the numerical analysis results from this study.

6. Author Contribution Statement

In the study carried out, Author 1 contributed to the formation of the idea, making the design and literature review, evaluating the results obtained, obtaining the materials used and examining the results, spelling and checking the article in terms of content.

7. Ethics Committee Approval and Conflict of Interest

"There is no conflict of interest with any person/institution in the prepared article"

8. List of Abbreviations

A_b	:	Cross section of the fin, m^2
CFD	:	Computational fluids Dynamics
g	:	Earth's gravity acceleration, m/s^2
h	:	Air convective heat transfer coefficient,
H	:	Characteristic length of the system, m
k_a	:	Thermal conductivity of the air, W/m.K
N	:	Total number of fins
N_{uH}	:	Nusselt number
N-S	:	Navier-Stokes
Pr	:	Prandlt number
PV	:	Photovoltaic
q_f	:	energy transferred through the whole fin,
Q_T	:	Total heat transfer, W
Ra	:	Rayleigh's number
T_∞	:	Air temperature, K
T_b	:	The temperature of the base of the fin, K
α	:	Thermal diffusivity of the fluid, m^2/s
β	:	Thermal expansion coefficient, K^{-1}
ΔT	:	Temperature difference, K
ν	:	Kinetic viscosity, m^2/s
ρ	:	Air density, kg/m^3

9. Ethical Statement Regarding the Use of Artificial Intelligence

No artificial intelligence-based tools or applications were used in the preparation of this study. The entire content of the study was produced by the author in accordance with scientific research methods and academic ethical principles.

10. References

[1] A. Shukla, K. Kant, A. Sharma, and P. H. Biwole, "Cooling methodologies of photovoltaic module for enhancing electrical efficiency: A review," Sol. Energy Mater. Sol. Cells, vol. 160, pp. 275–286, Nov. 2016.
[2] F. Ekinci, A. Yavuzdeğer, H. Nazlıgül, B. Esenboğa, B. D. Mert, and T. Demirdelen, "Experimental investigation on solar PV panel dust cleaning with solution method," Sol. Energy, vol. 237, pp. 1–10, Apr. 2022.
[3] R. Stropnik and U. Stritih, "Increasing the efficiency of PV panel with the use of PCM," Renew. Energy, vol. 97, pp. 671–679, Jun. 2016.
4] A. Yigit, N. Arslanoglu, and H. Gul, "Transient thermal modeling and performance analysis of photovoltaic panels," Environ. Prog. Sustain. Energy, vol. 42, no. 4, Nov. 2022.
[5] E. Cuce, P. M. Cuce, and T. Bali, "An experimental analysis of illumination intensity and temperature dependency of photovoltaic cell parameters," Appl. Energy, vol. 111, pp. 374–382, Jun. 2013.
[6] P. Dwivedi, K. Sudhakar, A. Soni, E. Solomin, and I. Kirpichnikova, "Advanced cooling techniques of P.V. modules: A state of art," Case Stud. Therm. Eng., vol. 21, p. 100674, Jun. 2020.
[7] G. Ömeroğlu, "Fotovoltaik - Termal (PV / T) Sistemin Sayısal (CFD) ve Deneysel Analizi," Fırat Univ. Müh. Bilim. Derg., vol. 30, no. 1, pp. 161–167, Mar. 2018.
[8] S. K. Marudaipillai, B. K. Ramaraj, R. K. Kottala, and M. Lakshmanan, "Experimental study on thermal management and performance improvement of solar PV panel cooling using form stable phase change material," Energy Sources Part A, vol. 45, no. 1, pp. 160–177, Aug. 2020.
[9] S. V. Hudișteanu et al., "Enhancement of PV panel power production by passive cooling using heat sinks with perforated fins," Appl. Sci., vol. 11, no. 23, p. 11323, Nov. 2021.
[10] W. Hammad et al., "Thermal management of grid-tied PV system: A novel active and passive cooling design-based approach," IET Renew. Power Gener., vol. 15, no. 12, pp. 2715–2725, May 2021.
[11] F. Al-Amri, F. Saeed, and M. A. Mujeebu, "Novel dual-function racking structure for passive cooling of solar PV panels – thermal performance analysis," Renew. Energy, vol. 198, pp. 100–113, Aug. 2022.
[12] A. Q. Jakhrani, A. R. Jatoi, and S. H. Jakhrani, "Analysis and fabrication of an active cooling system for reducing photovoltaic module temperature," Eng. Technol. Appl. Sci. Res., vol. 7, no. 5, pp. 1980–1986, Oct. 2017.
[13] A. M. A. Soliman, H. Hassan, and S. Ookawara, "An experimental study of the performance of the solar cell with heat sink cooling system," Energy Procedia, vol. 162, pp. 127–135, Apr. 2019.
[14] A. Monavari, J. Jamaati, and M. Bahiraei, "Thermohydraulic performance of a nanofluid in a microchannel heat sink: Use of different microchannels for change in process intensity," J. Taiwan Inst. Chem. Eng., vol. 125, pp. 1–14, Jun. 2021.
[15] M. Bahiraei et al., "Irreversibility characteristics of a modified microchannel heat sink operated with nanofluid considering different shapes of nanoparticles," Int. J. Heat Mass Transf., vol. 151, p. 119359, Jan. 2020.
[16] R. C. Adhikari, D. H. Wood, and M. Pahlevani, "Optimizing rectangular fins for natural convection cooling using CFD," Therm. Sci. Eng. Prog., vol. 17, p. 100484, Mar. 2020.
[17] R. M. Elavarasan et al., "An experimental investigation on coalescing the potentiality of PCM, fins and water to achieve sturdy cooling effect on PV panels," Appl. Energy, vol. 356, p. 122371, Nov. 2023.
[18] M. Krstic et al., "Passive cooling of photovoltaic panel by aluminum heat sinks and numerical simulation," Ain Shams Eng. J., vol. 15, no. 1, p. 102330, Jun. 2023.
[19] T. L. Bergman, F. P. Incropera, D. P. DeWitt, and A. S. Lavine, Fundamentals of Heat and Mass Transfer. New York, NY, USA: Wiley, 2012.
[20] C.-F. Yang et al., "Develop asymmetric, interference-free and excellent heat-dissipation CPU cooler," Case Stud. Therm. Eng., vol. 60, p. 104730, Jun. 2024.
[21] A. M. Elbreki et al., "Experimental and economic analysis of passive cooling PV module using fins and planar reflector," Case Stud. Therm. Eng., vol. 23, p. 100801, Dec. 2020.

[22] Z. Khattak and H. M. Ali, "Air cooled heat sink geometries subjected to forced flow: A critical review," Int. J. Heat Mass Transf., vol. 130, pp. 141–161, Oct. 2018.
[23] Y. Sheikh et al., "Enhancing PV solar panel efficiency through integration with a passive Multi-layered PCMs cooling system: A numerical study," Int. J. Thermofluids, vol. 23, p. 100748, Jul. 2024.
[24] N. Soares et al., "Can movable PCM-filled TES units be used to improve the performance of PV panels? Overview and experimental case-study," Energy Build., vol. 210, p. 109743, Dec. 2019.
[25] Z. M. Alaas, "The effects of temperature on photovoltaic and different mitigation techniques: a review," IEEE Access, p. 1, Jan. 2024.
[26] Q. Yang et al., "Enhancing concentrated photovoltaic power generation efficiency and stability through liquid air energy storage and cooling utilization," Sol. Energy, vol. 280, p. 112875, Aug. 2024.
[27] S. Kumari et al., "Efficiency enhancement of photovoltaic panel by heat harvesting techniques," Energy Sustain. Dev., vol. 73, pp. 303–314, Mar. 2023.
[28] L. Assiya, D. Aziz, and H. Ahmed, "Comparative study of P&O and INC MPPT algorithms for DC-DC Converter Based PV System on MATLAB/SIMULINK," in Proc. IEEE Int. Conf. Electron., Control, Optim. Comput. Sci. (ICECOCS), Dec. 2020, pp. 1–5.
[29] S. A. Mohamed and M. A. E. Sattar, "A comparative study of P&O and INC maximum power point tracking techniques for grid-connected PV systems," SN Appl. Sci., vol. 1, no. 2, Jan. 2019.
[30] M. A. Mahmood, K. Ishfaq, and M. Khraisheh, "Inconel-718 processing windows by directed energy deposition: a framework combining computational fluid dynamics and machine learning models with experimental validation," Int. J. Adv. Manuf. Technol., vol. 130, no. 7–8, pp. 3997–4011, Jan. 2024.
[31] P. A. D. Cruz et al., "Computational Fluid Dynamics (CFD) analysis of the heat transfer and fluid flow of copper (II) oxide-water nanofluid in a shell and tube heat exchanger," Digit. Chem. Eng., vol. 3, p. 100014, Feb. 2022.
[32] X. Y. Zhang et al., "Experimental investigation and CFD modelling analysis of finned-tube PCM heat exchanger for space heating," Appl. Therm. Eng., vol. 244, p. 122731, Feb. 2024.
[33] A. Pavlovic et al., "Thermal behavior of Monocrystalline silicon Solar cells: A Numerical and Experimental Investigation on the Module Encapsulation Materials," DOAJ, Jul. 2021.
[34] F. Ghafoorian et al., "Self-Starting improvement and performance enhancement in Darrieus VAWTs using auxiliary blades and deflectors," Machines, vol. 12, no. 11, p. 806, Nov. 2024.
[35] H. İ. Yamaç, A. Koca, and T. Yılmaz, "Using computational fluid dynamics for wave generation and evaluation of results in numerical wave tank modelling," Fırat Univ. J. Exp. Comput. Eng., vol. 1, no. 1, pp. 31–42, Jan. 2022.
[36] D. Kumar and B. Premachandran, "Effect of atmospheric wind on natural convection based solar air heaters," Int. J. Therm. Sci., vol. 138, pp. 263–275, Jan. 2019.
[37] T. T. Göksu, "Investigation of the effect of geometrical parameters and fluid properties of heat sinks on cooling by RSM method," Fırat Univ. J. Exp. Comput. Eng., vol. 3, no. 2, pp. 185–203, May 2024.
[38] N. A. Nalis et al., "Effects of Fin Height, Fin Thickness and Reynolds number on heat transfer enhancement of Flat-Plate thermal Collector: a numerical analysis," CFD Lett., vol. 15, no. 4, pp. 53–63, Feb. 2023.
[39] J. Jiang et al., "Evaluating the impacts of fin structures and fin counts on photovoltaic panels integrated with phase change material," Energy, vol. 283, p. 129143, Sep. 2023.